Pb-Free Solder: New Materials Considerations for Microelectronics Processing

Peter Borgesen, Thomas Bieler, L.P. Lehman, and E.J. Cotts

Abstract

A single printed circuit board includes thousands, sometimes even hundreds of thousands, of solder joints. The failure of even a single solder joint is usually enough to compromise the functionality of an electronic device or system. PbSn solder had been the standard material for these joints until various regulations around the world began to limit Pb use. SnAgCu and related alloys are quickly replacing PbSn, but much still needs to be understood and controlled. None of the paradigms for understanding the mechanical response of PbSn alloys is applicable to lead-free alloys. Much of the surprising behavior of SnAgCu solder arises from the complex and fascinating nature of its solidification behavior. In this article, the impact of solidification on the microstructure and therefore the mechanical properties of these solder joints will be addressed in the context of microelectronics processing. The need for better simulations of SnAgCu solder behavior will also be examined. Notably, modelers will have to account for a variety of new parameter dependencies not previously considered.

Overview

Most microelectronics products rely largely on solder for critical electronic and mechanical connections between individual devices and printed circuit boards.[1] A single board includes thousands, sometimes even hundreds of thousands, of solder joints. The failure of even a single solder joint is usually enough to compromise the functionality of an electronic device or system. Turning a device on often causes differential thermal expansions that can only be accommodated through significant plastic deformation of the solder joints and thus eventually leads to thermal fatigue. Joints must be able to survive mechanical loading caused by vibration, bending, or dropping. Predicting and controlling the reliability of the billions of solder joints formed in the automated manufacturing of a typical, high-volume product requires a thorough understanding of solder joint mechanical properties. In particular, the variability of the properties of solder must be understood and controlled.

Until recently, the vast majority of joints were formed using SnPb solder. There are many good reasons for this, including the high ductility and mechanical robustness of this material. A fortuitous benefit of this alloy is that the resulting joint properties are relatively insensitive to variations in composition, pad finishes, process parameters, and so on. This is critical to an industry that relies on the automated manufacturing of a tremendous number of electronics assemblies under a large variety of conditions. Despite these advantages, the electronic industry's successful dependence on SnPb solder is ending.[1]

A number of legislative initiatives around the world have called for the elimination of Pb from a range of products because Pb has deleterious health factors.[1] Curtailment of Pb use in different products in the United States began decades ago with the ban of Pb in products such as paint and gasoline. Companies in other countries (for instance, many in the Japanese electronics industry) began to introduce some Pb-free products years ago and realized significant commercial success.

As consumer demand for Pb-free products grew, the prohibition of Pb in products with a less immediate effect on the environment was considered. Notably, the European Union outlawed the use of Pb in most electronics produced after June 2006.[1] The result of this legislation is commonly referred to as the RoHS Directive, which stands for "the restriction of the use of certain hazardous substances in electrical and electronic equipment."[1] Although some products are initially exempted from this legislation, they will likely be subject to similar restrictions within a few years. Other products, such as military and medical ones, may technically remain exempt beyond that time, but eventually a loss of infrastructure will likely force them to switch to Pb-free soldering as well. Given this situation, much of the industry is converting to Pb-free solder on a worldwide basis.

A very large number of solder alloys have been developed and characterized as potential replacements of SnPb, but so far only near-eutectic SnAgCu, SnAg, and SnCu are acceptable to industry, with near-eutectic SnAgCu (SAC) compositions used most often. The eutectic-phase mixture (Sn-3.5wt%Ag-0.9wt%Cu) contains three room-temperature phases: Sn, Cu_6Sn_5, and Ag_3Sn.[2] These SAC alloys have serious drawbacks; notably, their higher melting points have led to a demand for more robust (and therefore expensive) packages and printed circuit boards. Pb-free SAC solder joints were initially believed to be more reliable in thermal cycling, but that assessment was based on test procedures that did not properly account for the very different properties of the Pb-free alloys. Most recently, there has been a growing recognition that the detailed properties of these new alloys tend to be much less reproducible under manufacturing conditions.

Whereas the two-phase SnPb solder can be modeled as a homogeneous and isotropic material, with reasonably well-known constitutive relations, accurate modeling of the mechanical behavior of a SnAgCu solder requires more careful accounting of its microstructure evolution.[3,4] The thermomechanical response of SnAgCu solder is dominated by that of the Sn, as opposed to

the softer Pb material in PbSn solder, and most SnAgCu solder joints are composed of essentially a few large Sn grains.[5–7] Given the marked anisotropies in the thermal expansion coefficient[8] and Young's modulus[9,10] of Sn, which vary by a factor of two or three with crystal direction, respectively, the morphology and orientation of the Sn grains are critical parameters in determining the thermomechanical response of SnAgCu solder joints.[11] Furthermore, Sn reacts to form intermetallic compounds with metals found in Pb-free solder joints (e.g., Ni, Au, Cu, and Ag), resulting in effects such as dispersion hardening. Thus, evolution of the precipitate microstructures, the Sn grains and their orientations, and the intermetallic compounds formed at solder/metallization interfaces must be considered.

The implementation of Pb-free solder in microelectronics has thus created significant new challenges.[1] The majority of manufacturers have already made the switch, but fully controlling and predicting the properties, performance, and reliability of these materials will require a fundamental understanding of the parameters that affect the thermomechanical response of SnAgCu solder joints.[12–14] In this article, the impact of solder solidification on the microstructure and, therefore, the mechanical properties of these solder joints is addressed. The need for better simulations of SAC solder behavior is also examined; notably, modelers must account for a variety of new parameter dependencies not previously considered.[15]

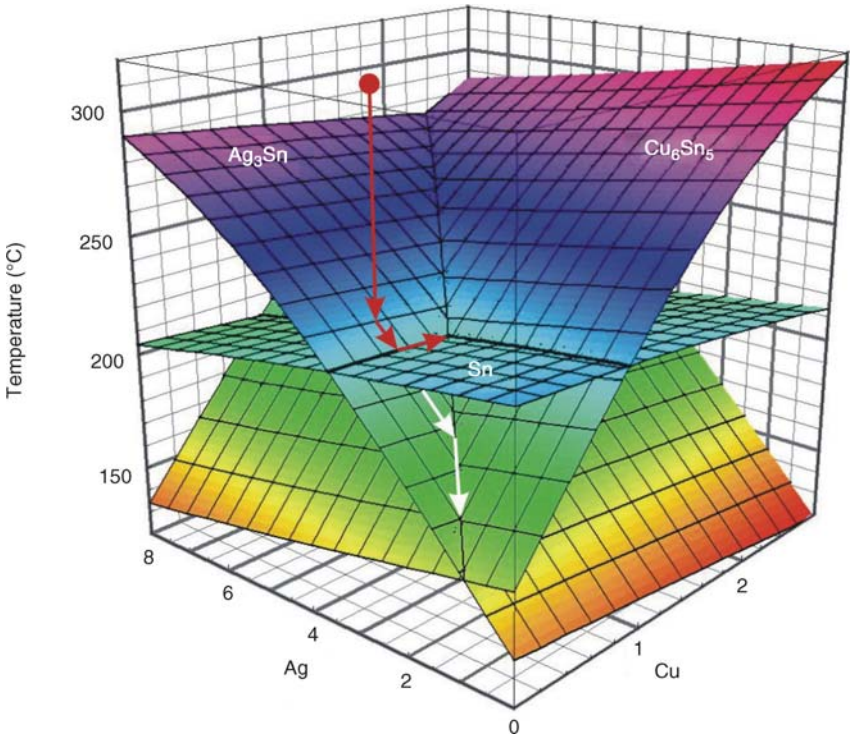

Figure 1. Three-dimensional rendering of the liquidus surfaces for the phases of the SnAgCu eutectic in the Sn-rich region of the Sn–Ag–Cu ternary phase diagram. Surfaces are extrapolated to temperatures below equilibrium to reflect possible undercooling (Sn, in particular, is prone to undercooling). An idealized composition/temperature trajectory for a typical SnAgCu solder is shown by red arrows; in this unlikely case, solidification occurs at the eutectic composition. A more realistic extension to this trajectory is shown by white arrows, reflecting the undercooling of Sn and the distillation of the undercooled Sn–Ag–Cu liquid toward pure Sn.

Impact of Solidification of SnAgCu Solder Joints on Microstructure

Much of the surprising behavior of SAC solder joints arises from the complex and fascinating nature of its solidification behavior. Sn undercools significantly in SAC solder joints, often dramatically affecting final solder joint microstructure. The nature of this solidification event is illustrated in Figure 1, a three-dimensional rendering of the liquidus surfaces for the Sn, Cu_6Sn_5, and Ag_3Sn phases that form upon cooling in this ternary system. A composition versus temperature cooling trajectory is superimposed upon these surfaces in Figure 1 for the Sn-3.9Ag-0.6Cu solder composition. An idealized trajectory for this material is shown in red, for the unlikely case of solidification occurring at near-liquidus temperatures, with the final solidification at the eutectic composition. A more realistic extension to this trajectory is shown in white, reflecting the observed dramatic undercooling of Sn and the distillation of the undercooling Sn-Ag-Cu liquid toward pure Sn. Significant Sn undercooling of 20°C–80°C in SnAgCu solder melts is generally observed, leading to significant ramifications on the final microstructure.

The large degree of undercooling of Sn in SAC solder joints results in some unusually large primary precipitates of Cu_6Sn_5 or Ag_3Sn, as shown in Figure 2. Fabrication of these solder joints involves heating the solder approximately 30°C above its melting point[16,17] for ~1 min. Although the melting temperatures of near-eutectic SnAgCu solder are approximately 217°C, larger Cu_6Sn_5 and Ag_3Sn precipitates in the solder sometimes do not finish dissolving after 1 min at 250°C. Thus, for realistic cooling rates (approximately 1°C/s), such unmelted, and hence primary, precipitates often have tens of seconds to grow in an undercooled Sn-based liquid matrix. As the degree of undercooling increases, the composition of the remaining liquid becomes more Sn-rich, following the white arrow trajectory in Figure 1. Thus, variations in the degree of undercooling, such as those associated with variations in solder volume, lead to significant variations

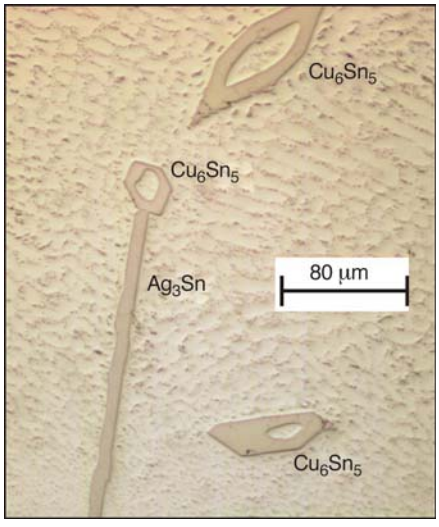

Figure 2. Optical micrograph of a Sn-3.9Ag-1.4Cu solder sample cooled at a rate of 0.1°C/s from a temperature of 250°C. The few primary precipitates are identified. Many much smaller secondary precipitates are visible in a Sn matrix.

in the volume and number of secondary precipitates and also the mean dendrite arm size (Figure 3).

After the Sn nucleates in the SAC melt, a sixfold, cyclic twinning growth process generally occurs, resulting in a very large, highly oriented Sn grain morphology.[11] Typical SnAgCu solder joints (Figure 4 and Figure 5b) have essentially only a few Sn grains, which grow dendritically from the same nucleus by a cyclic twinning process that results in only three orientations with a common [100] axis. Recalescence, the temperature rise associated with the release of the latent heat of fusion, limits or eliminates the nucleation of any other Sn crystals during the short growth time.

Influence of SnAgCu Microstructure on Pb-Free Solder Joint Properties

Sn Grains

There is clear evidence for a distinct dependence of cracking and failure of SnAgCu solder joints on variability in solder joint microstructures, in particular, on Sn grain size and orientation of the large Sn grains.[12,14,18,19] A straightforward example of this is provided in Figure 5, which reveals bright-field and crossed-polarizer views of the cross section of a solder joint that had undergone thermal cycling. As indicated by the discontinuities in the sample surface (see the arrows in Figure 5a), concentrated grain-boundary sliding deformation occurred across the middle of this solder ball. This is very different behavior from that of a near-homogeneous material, where maximum stress and deformation occur near the planar interfaces.

Deformation concentration along grain boundaries is correlated with the presence of large Sn grains, as illustrated in Figure 5b. This effect was also examined by Matin et al.,[18] who used crystal-based finite element modeling (FEM) methods to model thermomechanical stresses in polycrystalline microstructures with crystal-based anisotropic material properties. With temperature changes, von Mises stresses depended strongly upon the Sn grain orientation and morphology, leading to different out-of-plane strains near the solder/metallization interfaces and grain boundaries.[12]

Large variations in the failure rate of SAC solder joints can result from variations in the orientation of the Sn grains composing those joints. In one such study, the orientations of Sn grains in near-eutectic SAC solder joints were characterized after thermal cycling and correlated with the occurrence of fractures in these SAC solder balls (Figure 6).[19] Crack locations were noted and compared with the Sn grain orientation, as determined from electron backscattered diffraction orientation imaging scans. Samples with cracks had Sn grains primarily oriented with the Sn *c*-axis (the axis of highest coefficient of thermal expansion) parallel to the component and substrate planes. This reflects a clear dependence of the thermomechanical response of these solder joints on Sn grain orientation, as samples with this orientation have the greatest possible thermal expansion mismatch at the component interfaces (near which most cracks formed). Such a result directly contrasts with the typical behavior of SnPb solder joints, where the largest externally imposed stresses, at the package corners, are much more systematically correlated with initial failure locations.

Similar results have been observed in other studies. Optical examination of cross sections of a large number of individual SnAgCu solder joints after cycling revealed a greater variability from joint to joint in the rate of damage propagation than found in PbSn samples.[20] The locations of the

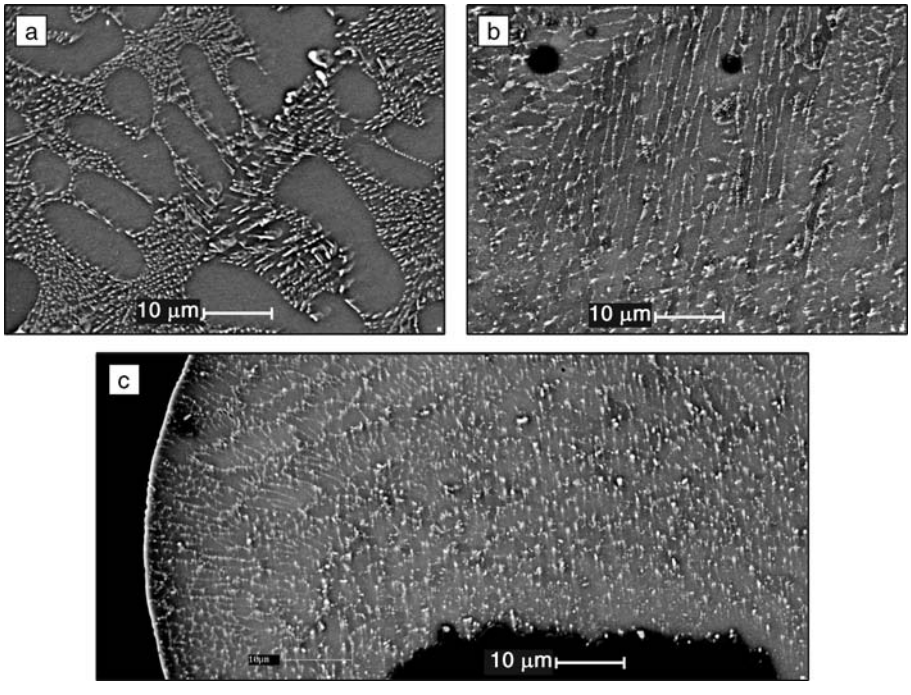

Figure 3. The number and size of secondary precipitates in the Sn matrix varies dramatically with undercooling (as determined by solder volume), even for very similar SnAgCu compositions. Backscatter composition-mode scanning electron microscope images of three commercially provided solder joints are shown. All images are displayed at identical magnification for comparison. Each image shows a portion of a different volume solder joint: (a) Sn-3.5Ag-1.0Cu solder volume of 0.001 mm^3 (ball grid array); (b) Sn-3.5Ag-1.0Cu volume of 0.01 mm^3 (chip-scale package); and (c) Sn-3.0Ag-0.8Cu solder volume of 0.23 mm^3 (flip chip). The mean dendrite arm widths were measured to be 6, 1.8, and 1.1 μm for samples in (a), (b), and (c) respectively. (From Reference 26.)

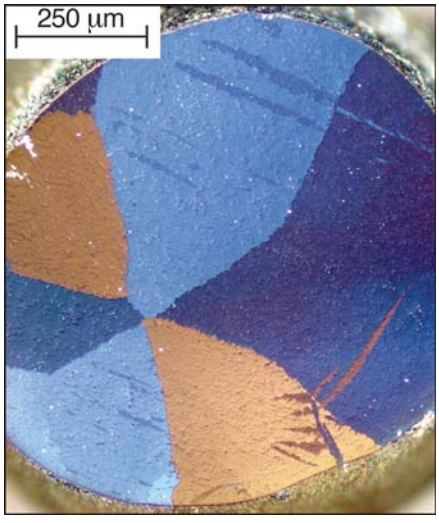

Figure 4. Optical micrograph with crossed polarizers of a Sn-1.65Ag-0.59Cu sample, cooled at a rate of 0.01°C/s from a temperature of 250°C. This more clearly corresponds to a sixfold cyclic twinning (across [101] planes) growth mechanism.

solder balls that revealed cracking in SnAgCu arrays varied more than in PbSn arrays.[20] Furthermore, the observed mean value of time to failure can vary significantly, if not dramatically, with variations in thermal history. Hence, Sn crystal orientation can have a large impact on damage evolution in Pb-free solders. Thus it is quite difficult for practitioners to predict the relationship between accelerated thermal cycling tests and behavior in service.

Impact of Dispersion/Precipitation Evolution on Hardness, Strength, and Creep Properties

None of the paradigms for understanding the mechanical response of SnPb alloys are applicable to Pb-free alloys.[21–30] For instance, crack propagation has been observed along large primary precipitates (see Figure 7) in SAC solder joints. Such precipitates are not found in SnPb alloys. In general, as solders operate at temperatures above half their melting temperature, mechanical properties such as hardness and strength are best understood in terms of creep or hot deformation. The creep properties of SAC solders are dominated by those of precipitate-hardened Sn, which exhibits a very different behavior than SnPb solder. Secondary precipitates (e.g., Cu_6Sn_5 and Ag_3Sn) are the principal hardening agents in SnAgCu Pb-free solders. These Sn-based SAC-based alloys show stress exponents from 5–9, implying that creep is controlled by dislocation climb impeded by precipitates, with low activation energies commonly attributed to pipe diffusion.[31,32]

Because the volume fraction of intermetallic compound precipitates in these Sn-based alloys is small (~5%), the morphology (size, and hence spacing, or number per unit volume) of the precipitates has a large impact on the creep properties. This morphology is extremely sensitive to details of composition, cooling rate, solidification temperature, annealing times, and annealing temperatures (see Figure 3), all of which cause significant variability in mechanical responses of the solder to stress. Large solder balls tend to experience relatively modest undercooling so they produce relatively coarse secondary precipitates, whereas small solder balls tend to have deeper undercooling and produce much finer secondary precipitates.[33] Given that the tensile strength of SnAgCu alloys increases with increasing cooling rate because of the production of finer and more closely spaced precipitates, both the cooling rate and the ball diameter affect the strength.[34–36]

The microstructure and resulting solder joint properties can also vary strongly with subsequent aging, annealing, or thermal cycling.[37] The as-solidified microstructure will coarsen, even at room temperature, reducing the hardness and strength of the solders.[33,35,37] After water quenching and aging at room temperature, the tensile strength of cast bars decreased from 60 MPa to 45 MPa after 35 days.[26] The coarsening rate of finer structures is fast because of the smaller diffusion distances between precipitates and the higher chemical potential of small radius of curvature precipitates. Thus, finer structures will be harder at first and soften more quickly in response to mechanical or thermal energy input. The rate of coarsening in thermal cycling can be enhanced in comparison with isothermal aging because of stress-enhanced diffusion, as well as changes in the solubility limit of Sn with temperature that enable partial dissolution of precipitates at elevated temperature. Considering all of the variables that affect the microstructure and thus the thermomechanical properties of

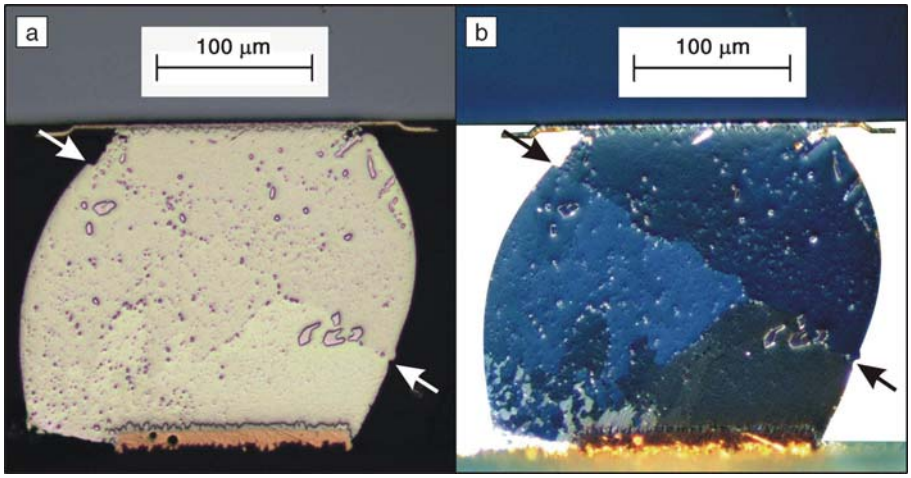

Figure 5. Optical micrographs of a cross section of Sn-3.5Ag-1.0Cu solder joint thermally cycled between 0°C and 100°C. (a) Bright-field image and (b) image taken with crossed polarizers. Different Sn grains are delineated. The arrows indicate surface discontinuities associated with grain-boundary sliding along a Sn crystal boundary that subtends the solder joint (between the arrows).

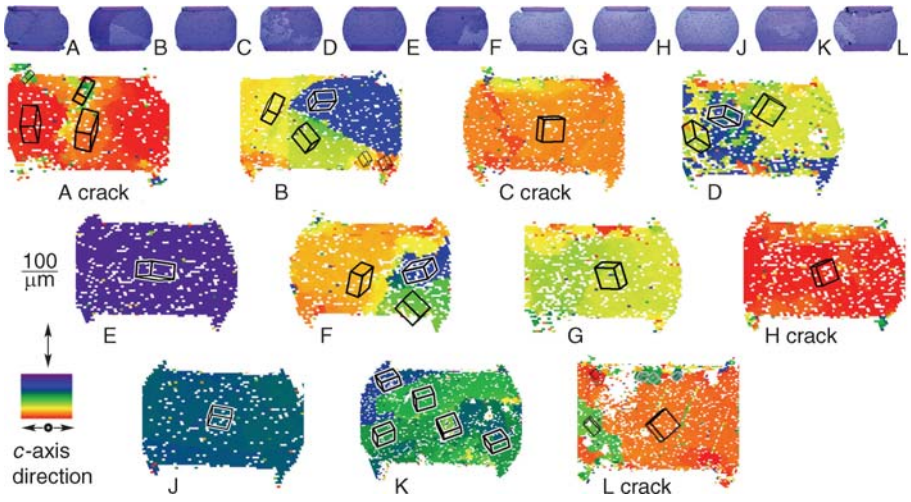

Figure 6. Maps of the orientation of the *c*-axis of Sn for a row of 11 cross-sectioned SnAgCu solder balls in a thermomechanically cycled package. The orientations of the *c*-axis are indicated by color (see key in figure), with purple corresponding to the *c*-axis perpendicular to component and board, and orange-red corresponding to the *c*-axis parallel to component and board. Cracks were observed in four of the optical micrographs; these samples are labeled "crack." (From Reference 29.)

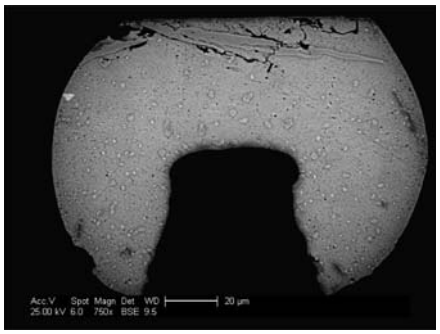

Figure 7. Flip-chip solder joint after thermal cycling. Early failure along (and through) a large Ag_3Sn platelet.

SnAgCu, it is understandable that practitioners experience surprises with this material.[38]

Attempts to Control SnAgCu Solder Joint Microstructure

A number of efforts are underway to alleviate some of the effects outlined in the previous sections, for instance, by controlling the solidification of Sn during solder joint fabrication. Thus many studies[39–41] have examined the effect of other alloying elements (such as Ni or Zn at the 0.05%–0.5% level) in SnAgCu. Zn is very effective in reducing the degree of undercooling of Sn in SnAgCu and thus reducing some of the associated variability of the solder microstructures and reducing the dissolution rate of Cu pads. Unfortunately, even with enhanced nucleation of Sn, only one or a very few Sn grains were observed in these solder joints. Furthermore, Zn forms different intermetallic compounds at the contact pads when it reacts with Cu, Ni, and Au. Zn is particularly effective in preventing occasional voiding in the Cu_3Sn layer on Cu pads, so interest in this element remains high. The addition of Ni has a lesser effect on undercooling and intermetallic formation, but it does modify the interfacial intermetallic thicknesses and harden the solder slightly. Ni may enhance the formation of more uniformly spaced $(Cu,Ni)_6Sn_5$ precipitates that may reduce microstructural variability.[42] However, Ni apparently enhances voiding in the Cu_3Sn. Finally, a decrease in the Ag content of SnAgCu can limit the maximum sizes of primary precipitates (large precipitates can result in strongly variable effects on crack propagation). Nevertheless, until recently, the most common alloy had 3.8–4.0 wt% Ag, but there is an ongoing trend toward lower Ag content (perhaps as low as 1 wt%), because of the associated greater ductility. Eutectic SnCu is a likely favorite for flip-chip applications.

Toward the Development of More Realistic Constitutive Relations

A better understanding and control of SnAgCu microstructures is needed before rules for controlling it can be used by designers. Both modeling and experimental investigations of the mechanical response of solder joints as a function of solder joint microstructure, in particular, Sn grain morphology and all the factors that influence it, are necessary. To date, isotropic phenomenological models exist that can treat solder alloys in an average manner.[43,44] Such models are valuable for system-scale design purposes, but they cannot capture the heterogeneous behavior observed in individual solder joints. To effectively predict failure processes in a particular joint (and thus have the ability to predict early failures), a more physically based anisotropic material model is needed, which includes details of operative slip systems and recovery processes. Models of individual joints with realistic microstructures could have boundary conditions imposed, based on the displacement history determined from a system-scale computation that uses scalar (average) properties to provide boundary conditions for deformation of a specific joint.[45] Although there is some identification of crystal-scale properties,[46–48] much work is still needed to identify and express slip system–based deformation, recovery, grain-boundary sliding, and recrystallization processes in quantitative forms at the crystal scale. Attempts to model and interpret results require substantial simplifications that must be interpreted with full cognizance of these assumptions. Most importantly, it is clear that forays in modeling this complex crystal system must be attempted and that experimental data needed for constitutive modeling at the grain scale must be obtained, analyzed, and understood before reliability models based upon physical understanding can be developed.

Conclusion

The introduction of Pb-free, SnAgCu solders into the marketplace will continue to cause unanticipated failures that cannot be predicted by existing phenomenological models or accelerated tests. It is important to assess such failures rigorously and to identify the contributions of precipitate morphology, interface evolution, grain-boundary characteristics, and Sn crystal orientation to failure (all of which depend on the solidification path). It is also important to further identify worst-case scenarios for SnAgCu solder joints, such as the *c*-axis parallel to the interface (as shown in Figure 6), and to determine the statistical probability of forming worst-case microstructures during manufacturing. To the extent that worst-case microstructures cannot be eliminated, lifetime can only be accurately assessed if these microstructures are included in models. This requires the development of physically based solidification and deformation models as well as the ability to reproduce the worst-case scenarios intentionally for testing. Fundamental experimental research is central to support the development of such models and capabilities.

Acknowledgments

Support from the National Science Foundation grant DMI0218129 is gratefully acknowledged. Contributions to this article from Pericles Kondos, Julie Nucci, and Yan Xing are gratefully acknowledged. Thomas R. Bieler is grateful for sabbatical support from Michigan State University and the Max-Planck-Institut für Eisenforschung in Düsseldorf, Germany.

References

1. K.J. Puttlitz, K.A. Stalter, Eds. *Handbook of Lead-Free Solder Technology for Microelectronic Assemblies* (Marcel Dekker, New York, 2004), and related Internet links: IPC Compliance Web Site, http://leadfree.ipc.org/RoHS_3–2-1–4.asp; EC Environment Policy, Waste Electrical and Electronic Equipment, http://ec.europa.eu/environment/waste/weee_index.htm; U.K. Department of Trade and Industry Web Site, EC Directive on Waste Electrical and Electronic Equipment, www.dti.gov.uk/innovation/sustainability/weee/page30269.html; Grace Compliance Specialist Web Site, www.grasplc.com/China%20RoHS.php/.
2. K.W. Moon et al., *J. Electron. Mater.* **29**, 1122 (2000).
3. J.-P. Clech, *MicroMater. Nanomater.* **3**, 144 (2004).
4. R. Darveaux, K. Banerji, A. Mawer, G. Dody, in *Ball Grid Array Technology*, J.H. Lau, ed. (McGraw-Hill, New York, 1995) pp. 379–442.
5. L.P. Lehman et al., *J. Electron. Mater.* **33** (12), 1429 (2004).
6. A.U. Telang, T.R. Bieler, *JOM* **57**, 44 (2005).
7. A.U. Telang, T.R. Bieler, S. Choi, K.N. Subramanian, *J. Mater. Res.* **17**, 2204 (2002).
8. D.R. Frear, *J. Met.* **48**, 49 (1996).
9. D.G. House, E.V. Vernon, *Br. J. Appl. Phys.* **11**, 254 (1960).
10. J.A. Rayne, B.S. Chandrasekhar, *Phys. Rev.* **120**, 1658 (1960).
11. K.N. Subramanian, J.G. Lee, *J. Mater. Sci.–Mater. Electron.* **15**, 235 (2004).
12. S.B. Park, R. Dhakal, L.P. Lehman, E.J. Cotts, in *Proc. ASME InterPACK* (San Francisco, CA, 2005).
13. D.R. Frear, J.W. Jang, J.K. Lin, C. Zhang, *J. Met.* **53**, 28 (2001).
14. D.W. Henderson et al., *J. Mater. Res.* **19** (6), 1608 (2004).
15. Special Issue on Lead-Free Solders and Processing Issues in Microelectronics Packaging, *J. Electron. Mater.* **32**, 1359 (2003).
16. K. Zeng, K.N. Tu, *Mater. Sci. Eng. R* **38**, 55 (2002).
17. A. Zribi et al., *J. Electron. Mater.* **30**, 1157 (2001).

18. M.A. Matin, E.W.C. Coenen, W.P. Vellinga, M.G.D. Geers, *Scripta Mater.* **53**, 927 (2005).
19. T.R. Bieler et al., *Proc. 56th Electronic Components Technology Conf.* (2006) p. 6.
20. L.P. Lehman et al., *Proc. 55th Electronic Components Technology Conf.* (2005) p. 674–681.
21. W.C. Luoa et al., *Mater. Sci. Eng. A* **396**, 385 (2005).
22. K. Kim, K. Suganuma, J. Kim, C. Hwang, *J. Met.* **56**, 39 (2004).
23. A.U. Telang et al., *J. Electron. Mater.* **33** (12), 1412 (2004).
24. F. Ochoa, X. Deng, N. Chawla, *J. Electron. Mater.* **33** (12), 1596 (2004).
25. K.P. Wu, N. Wade, S. Yamada, K. Miyahara, *Z. Metallkd.* **95** (3), 185 (2004).
26. Q. Xiao, L. Nguyen, W.D Armstrong, *Proc. 54th Electronic Components Technology Conf.* (2004) p. 1325–1332.
27. R.L.J.M. Ubachs, P.J.G. Schreurs, M.G.D. Geers, *IEEE Trans. Components Packaging Technologies* **27** (4), 635 (2004).
28. S. Jadhav, T.R. Bieler, K.N. Subramanian, J.P. Lucas, *J. Electron. Mater.* **30**, 1197 (2001).
29. S. Choi et al., *J. Met.* **53**, 22 (2001).
30. A.U. Telang, T.R. Bieler, M.A. Crimp, *Mater. Sci. Eng. A* **421** (1–2), 22 (2006).
31. J. Weertman, *Trans. Am. Inst. Min. Eng.* **218**, 207 (1960).
32. M.D. Mathew, Y. Hang, S. Movva, K.L. Murty, *Metall. Mater. Trans.* **01.36A** (1), 99 (2005).
33. R. Kinyanjui, L.P. Lehman, L. Zavalij, E. Cotts, *J. Mater. Res.* **20**, 2914 (2005).
34. K.S. Kim, S.H. Huh, K. Suganuma, *J. Alloys Compd.* **352**, 226 (2002).
35. F. Ochoa, X. Deng, N. Chawla, *J. Electron. Mater.* **33** (12), 1596 (2004).
36. K.P. Wu, N. Wade, S. Yamada, K. Miyahara, *Z. Metallkd.* **95** (3), 185 (2004).
37. I. Dutta, D. Pan, R.A. Marks, S.G. Jadhav, *Mater. Sci. Eng. A* **410–11**, 48 (2005).
38. S.K. Kang et al., in *Proc. 54th Electronic Components Technology Conf.* (2004) p. 661–667.
39. J.G. Lee, K.N. Subramanian, *Soldering Surf. Mount Technol.* **17** (1), 33 (2005).
40. S.K. Kang et al., *J. Electron. Mater.* **35** 479 (2006).
41. I.E. Anderson, J.L. Harringa, *J. Electron. Mater.* **33**, 1485 (2004).
42. J.C. Gong, C.Q. Liu, P.P. Conway, V.V. Silberschmidt, *Mater. Sci. Eng. A* **427** (1–2), 60 (2006).
43. R. Darveaux, K. Banerji, *IEEE Trans. Components, Hybrids, Manuf. Technol.*, **15** (6), 1013 (December 1992).
44. Y. Wei et al., *J. Electron. Packaging* **126** 367 (2004).
45. J. Gong, C. Liu, P.P. Conway, V.V. Silberschmidt, *Comput. Mater. Sci.* (2007) in press, www.sciencedirect.com.
46. H. Rhee, K.N. Subramanian, *Soldering Surf. Mount Technol.*, **18** (1), 19 (2006).
47. C. Kanchanomai, Y. Miyashita, Y. Mutoh, S.L. Mannan, *Mater. Sci. Eng. A* **345** 90 (2003).
48. S. Terashima, K. Takahama, M. Nozaki, M. Tanaka, *Mater. Trans. JIM* **45** (4), 1383 (2004).

Thomas Bieler *is an associate professor in the Department of Chemical Engineering and Materials Science at Michigan State University. He earned a BA degree in applied mechanics from the University of California, San Diego, in 1978 and an MS degree in ceramic engineering at the University of Washington, Seattle, in 1980. Bieler worked as a member of the technical staff in the Applied Mechanics Division at Sandia National Laboratory in Livermore from 1980 to 1985, and completed his PhD degree in materials science at the University of California, Davis, in 1989. He has worked at Michigan State University since 1989.*

Bieler can be reached by e-mail at bieler@egr.msu.edu.

Peter Borgesen *is the manager of the Area Array Consortium at Unovis Solutions in Kirkwood, N.Y. Borgesen earned his PhD degree in physics from the University of Aarhus in Denmark. Before joining the SMT Laboratory at Universal Instruments Corp. in 1994, Borgesen worked at national laboratories in Denmark and Germany as well as in the Materials Science Department at Cornell University. In 2006, SMT was combined with other divisions from Universal and Hover-Davies to form Unovis Solutions. The Area Array Consortium is an international group of companies from across the industry sponsoring research conducted by the Advanced Process Lab at Unovis Solutions on automated first- and second-level microelectronics assembly processes and reliability.*

Borgesen can be reached by e-mail at borgesen@unovis-solutions.com.

Eric J. Cotts *serves as chair of the Physics Department and co-director of the Materials Science Program at Binghamton University, State University of New York. He received his BS degree from Cornell University in 1978 and his PhD degree from the University of Illinois at Urbana-Champaign in 1983. Cotts studies transport phenomena at small length scales, with a focus on basic problems with direct relevance to microelectronics.*

Cotts can be reached at tel. 607-777-4371 and e-mail ecotts@binghamton.edu.

Lawrence P. Lehman *is the lab manager of a materials characterization laboratory at Binghamton University, State University of New York. He received his BS degree in physics at Edinboro University of Pennsylvania and his PhD degree in materials science at the University of Notre Dame in South Bend, Indiana. He worked at Argonne National Laboratory, Materials Science Division; IBM, Printers Division and Microelectronics Division; and most recently at Binghamton University's Physics Department. Lehman's current research interests include the microstructure and crystallography of Pb-free solders.*

Lehman can be reached at Binghamton University, State University of New York, Physics Dept., Sci-2, PO Box 6000, Binghamton, NY 13902-6000, USA; tel. 607-437-1880 and e-mail lplehman@binghamton.edu.